Microscopic self-consistent theory of Josephson junctions including dynamical electron correlations

P Miller[1,2] **and J K Freericks**[1]

[1] Department of Physics, Georgetown University, Washington, DC 20057-0995, USA
[2] Department of Physics, Brandeis University, Waltham, MA 02454, USA

E-mail: freericks@physics.georgetown.edu

Abstract

We have developed a rapid computational algorithm that allows for a
fully self-consistent solution of the three-dimensional Bogoliubov–de Gennes
equations for a Josephson junction. This microscopic model is appropriate
for short-coherence-length superconductors, Josephson junctions with strongly
correlated proximity-coupled weak links and systems where the barrier
thickness is the same order of magnitude as the coherence length. This is a
regime that is usually not described by the highly successful analytic theories
of Josephson junctions developed over the past 35 years. The formalism is
applied to the simplest possible model as an example, but can easily incorporate
correlation effects (via the dynamical mean field theory) with relatively little
extra cost. We examine current–phase relations, effects of non-magnetic
impurities, interfacial scattering and the local density of states within the
barrier. This last 'theoretical spectroscopy' shows the evolution of Andreev
bound states in the presence of a Josephson current, illustrating the expected
Doppler shift. We also calculate the figure of merit, $I_c R_N$, and find that our
self-consistent solutions produce a variation of this product, which can be
dramatically increased for coherent SNSNS junctions which have an additional
thin superconducting layer within the normal-metal region.

1. Introduction

Some of the most successful and promising electronics applications of superconductors involve
Josephson junctions, where two superconducting regions are coupled through a barrier region,
made from a non-superconducting material [1]. The drive to make electronic devices using
Josephson junctions has been motivated by their naturally high operating frequencies, far in
excess of the speeds obtainable in standard silicon technology. The operational frequency
of an ideal Josephson junction using rapid single flux quantum (RSFQ) logic is $I_c R_N e/\hbar$,
where I_c is the critical current, and R_N is the normal state resistance of the junction [2–6]
(RSFQ logic requires that the I–V characteristics be nonhysteretic). Hence a maximum value

of the product, $I_c R_N$ leads to optimal performance for nonhysteretic junctions. At present, low-temperature superconductors have been used to produce junctions with $I_c R_N$ products up to 1 mV, and operational speeds reaching 770 GHz [6, 7], while junctions of high-temperature superconductors have achieved $I_c R_N$ products reaching from 1 mV to $\approx$20 mV [8, 9]. There are two strategies to achieve high operating speed for RSFQ logic with low-T_c superconductors: (i) by reducing the area of the junction and the thickness of the insulating barrier, very high-speed self-shunted junctions can be made that have nonhysteretic I–V characteristics [10], and (ii) by splitting the insulating layer and separating it by a normal layer (so-called SINIS junctions) one can achieve high speeds with somewhat larger junction sizes [11]. As the junction area is made smaller, a simple estimate of the resistance needed to achieve good junction characteristics lies close to the metal–insulator transition region, where correlations within the barrier material become increasingly important. Indeed, it has been suggested [12] that an optimum value of the $I_c R_n$ product would be reached when the barrier material is close to a metal–insulator transition, so that the system is near the cross-over from an SNS to an SIS junction. This is a regime that lies outside of the known analytic limits of diffusive, short (or long) junctions that have been studied for many years. In order to investigate such non-trivial barrier materials, we develop a microscopic model of a Josephson junction, which self-consistently incorporates the dynamical correlation effects of the electrons in calculating the conductance of the junction and the critical current.

Our model is also appropriate for ballistic junctions that have relatively pure barrier regions so that the extent of the barrier is smaller than its mean-free path but larger than (or on the order of) its proximity-effect-induced superconducting correlation length. This work also has relevance as a first approach to high-T_c superconductor junctions where the coherence length is relatively short and typically on the order of the size of the barrier region. (High-T_c superconductors also have many geometrical effects associated with the d-wave order parameter, but we have decided to separate those geometric issues from the quantum-mechanical issues brought up by barrier sizes on the order of the coherence length. Here we consider only s-wave short-coherence-length superconductors.)

Much experimental work has progressed on these systems recently, with a concentration on niobium–indium arsenide–niobium junctions or niobium–silicon–niobium junctions. Recent work includes an examination of subgap structures and current deficits [13], quasiparticle reflection effects and spikes in the conductance [14], an investigation of a tunable junction that can be altered from an ordinary junction to a π-junction by driving the barrier into a nonequilibrium state via a transverse electrical current [15], and a study of critical currents in junctions with barrier sizes on the order of the coherence length [16]. This contribution will address only equilibrium and linear-response properties of the microscopic model for Josephson junctions, but our work can be extended to examine nonequilibrium effects as well.

Our technique provides different information than the conventional analytic and numeric approach for diffusive junctions. The conventional approach seeks to describe junctions through a series of parameters characterizing the different components of the junction (such as the superconducting transition temperature, coherence length, normal state resistivity, barrier transparency, suppression parameter etc); some of the parameters can be determined from independent measurements; others are adjusted to provide a phenonomenological fit with experiment. Our approach is to start from a completely microscopic model that involves only local interaction parameters (such as the hopping integral between two atomic sites, the screened Coulomb interaction, the impurity scattering strength etc) and to derive all of the relevant phenomonological parameters of the conventional theory from the microscopic model. Such an approach provides an alternative framework that complements the conventional approach and provides an understanding of how modifying microscopic elements of a junction

affects the phenomonological parameters and thereby the junction properties.

The main qualitative characteristics of a Josephson junction can be understood by just considering two superconductors coupled together with a single, energy-independent transparency. The dc Josephson effect, of a direct supercurrent through the junction at zero external voltage, and the ac Josephson effect, of an oscillating current at finite voltage, were both predicted from such a simple model [1]. Further details of the $I-V$ characteristics, such as excess current and sub-harmonic gap structure due to Andreev bound states, were explained [17, 18], by matching boundary conditions across a step-function in the superconducting potential, and including an adjustable scattering potential at the interfaces [19, 20]. Analytic calculations have been performed to provide current–phase relationships [21–25], representing the barrier as a single scattering potential with no spatial extent. In this contribution we compare these traditional approaches with a microscopic model that includes self-consistency of the superconducting order parameter through a barrier that has a finite extent, to examine what the effects of self-consistency are on these theoretical models. For example, the analytic results predict that the maximum of the current–phase relation always lies at a phase difference lying between $\pi/2$ and π, while a one-dimensional model [26] showed that self-consistency modified the current phase relation so that the maximum always occurred at a phase difference less than $\pi/2$. Here we find that a three-dimensional model can have a maximum of the current–phase relation occuring anywhere in the range from 0 to π.

In this paper, we present a method for studying the effects of the barrier region on the strength of superconductivity it can support, and hence on the supercurrent it can maintain. Effects of electron correlations are incorporated within the dynamic mean field theory [27–30], which leads to a local, frequency-dependent self-energy, which we allow to vary from one plane to the next, while assuming it to remain constant within individual planes. Hence the three-dimensional system becomes inhomogeneous in the one dimension where the current flows (which we label the z-direction). We model the system with two sets of N_{SC} planes of superconducting material coupled each on one side to the bulk superconductor, and on the other side sandwiching N_b planes of barrier material as depicted in figure 1. The total number of planes modelled self-consistently is $2N_{SC} + N_b = N$. We note that while in this paper we concentrate on applying the method to Josephson junctions, our method would also be applicable to theoretical studies of correlated electrons at surfaces, single interfaces, or multiple interfaces, as first demonstrated by Potthoff and Nolting [31].

An important advantage of our scheme is that the different (material specific) microscopic models that best describe any particular material can be coupled together across the planes. Hence a superconductor with electron–phonon coupling described by a Holstein model [32] (or even using a materials-specific $\alpha^2 F$ in Migdal–Eliashberg theory) can be connected to a metallic region with impurities described by the Falicov–Kimball model (or a correlated Hubbard model), and so on. The local self-energy for each plane is calculated independently, according to the model best suited to the particular material. Once a set of local self-energies are evaluated for each plane, the Green functions are calculated by finding the inverse of an infinite matrix which includes planes of bulk superconductor extending in the positive and negative z-direction. The inversion process, which is made tractable by a continued-fraction representation, couples all of the different planes together, such that a change in the self-energy on one plane affects the local interacting Green functions on all other planes, particularly those nearby in real space.

In order for a supercurrent to flow, a phase gradient must be applied to the superconductor and across the barrier region. The critical current, I_c, is reached, when the planes with the lowest superconducting order, typically at the centre of the barrier region, can no longer support the necessary phase gradient to maintain current continuity. In our model, we find the supercurrent
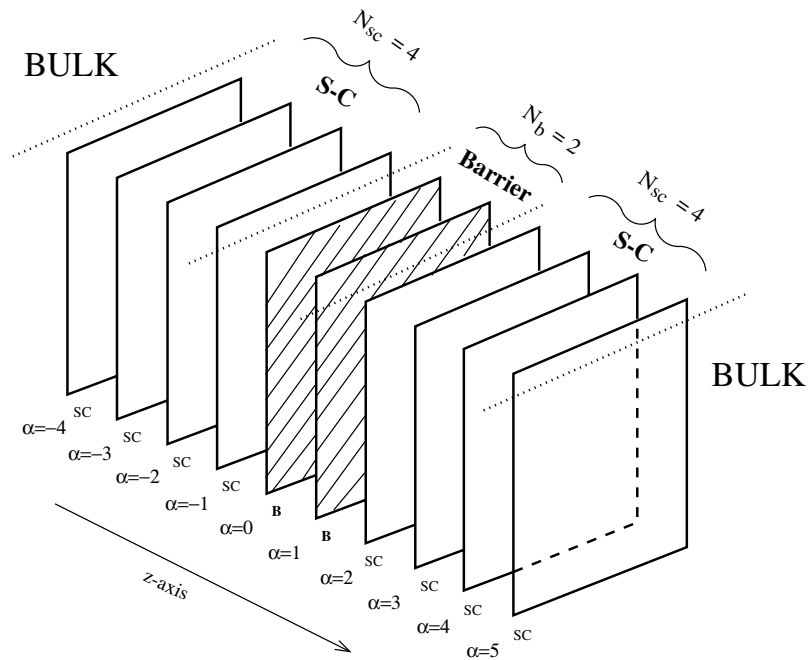
Figure 1. Microscopic stacked planar geometry of a Josephson junction. The sandwich of $N = 10$ planes; $N_{sc} = 4$ superconducting planes coupled to a bulk superconductor on the left and $N_b = 2$ barrier planes on the right, followed by a further $N_{sc} = 4$ superconducting planes coupled to another bulk superconductor on the right. The system is allowed to have spatial inhomogeneity only within the N modelled planes, but the calculations are always for an infinite system.

as a function of phase variation across the barrier, by solving the system self-consistently at each set of phases. The self-consistency is crucial [26, 33–35], as the existence of a current flow affects the value of the superconducting order parameter, both inside and outside the barrier region.

Section 2 contains a detailed description of our method, including the physical approximations used, and the general computer algorithm. We provide these details here because our computational techniques are so different from the conventional analytic theories based on Eilenberger or Usadel equations. In section 3 we analyse the current–phase relationships of our results in terms of an effective transparency of the barrier. The results presented in section 4 demonstrate the efficacy of the method to solve some simple models of Josephson junctions, using the Bogoliubov–de Gennes equations, where we demonstrate the effects of self-consistency, in particular on the superconducting order and electron density. Section 5 includes the results for barriers with impurity scattering, with a description of the calculations of normal-state resistance, and results of resistance and $I_c R_N$ products. We conclude in section 6 with some comments on the results, and suggestions of other situations well suited to our model.

2. Method

Our method consists of two stages. First, we determine the properties of the bulk boundary regions for a uniform system. When no current flows in the bulk (homogeneous)

superconductor, dynamical mean field theory [27–30] is employed to determine the local self-energy, using the local approximation. When a uniform current is flowing, one must include a uniform phase variation in the superconducting order parameter, $\Delta(z)$, for the bulk system. Next, we solve the inhomogeneous problem self-consistently by iteration, for a number of planes, N, coupled on either side to the uniform bulk solution (this strategy allows us to avoid any ambiguity that might enter by assuming a particular form for the boundary conditions at the interfaces). That is, giving the plane an index, α, and defining the central link of the junction to be between planes $\alpha = 0$ and $\alpha = 1$, we include N_b barrier planes, surrounded by N_{sc} self-consistently calculated superconductor planes on each side, such that $N = N_b + 2N_{sc}$ and planes with index, $\alpha < 1 - N/2$ or $\alpha > N/2$ are invariant homogeneous bulk planes (see figure 1). Typically, we solve systems with $N_{sc} = 30$, which is significantly larger than the coherence length for our bulk superconductor ($\xi = \hbar v_F / (\pi \Delta) \approx 4a$, where a is the lattice spacing). We observe that, except when very close to T_c, the superconducting order has completely healed from its disruption at the interface, by the time we reach the planes at the bulk superconductor boundary (planes with $\alpha \approx \pm N/2$).

We describe the system with the following tight-binding model:

$$\hat{H} = \sum_{i,j,\sigma} t_{ij} \hat{c}_{i\sigma}^\dagger \hat{c}_{j\sigma} + \sum_i U_i \left(\hat{c}_{i\uparrow}^\dagger \hat{c}_{i\uparrow} - \frac{1}{2} \right) \left(\hat{c}_{i\downarrow}^\dagger \hat{c}_{i\downarrow} - \frac{1}{2} \right) + \sum_{i,\sigma} U_i^{FK} \hat{c}_{i\sigma}^\dagger \hat{c}_{i\sigma} w_i \tag{1}$$

where $\hat{c}_{i\sigma}^\dagger$ and $\hat{c}_{i\sigma}$ are fermionic operators which respectively create and destroy an electron of spin σ in a single Wannier (tight-binding) state on the lattice site i;

$$t_{ij} = \begin{cases} \epsilon_\alpha & \text{if } i = j \text{ on plane } \alpha \\ -t_\alpha & \text{if } i \text{ and } j \text{ are neighbouring sites on the same plane, } \alpha \\ -\sqrt{t_\alpha t_{\alpha'}} & \text{if } i \text{ and } j \text{ are neighbouring sites on consecutive planes, } \alpha \text{ and } \alpha' \\ 0 & \text{otherwise} \end{cases}$$

with $-t_\alpha$ the overlap or hopping integral for the αth plane, ϵ_α the local site energy, U_i the renormalized on-site, Hubbard interaction energy, U_i^{FK} the impurity potential and $w_i = 1$ if there is an impurity on site i, and $w_i = 0$ otherwise. The magnitude of the hopping integral in the superconducting region, t, is constant, and defines our energy scale for the entire system ($t = 1$). Note that this hopping integral should not be confused with the effective matrix element or transfer amplitude of a tunnelling Hamiltonian, typically used to describe Josephson junctions, but is instead the overlap integral between atomic orbitals centered on neighbouring lattice sites.

In all results that we present here, the superconducting region has an attractive Hubbard interaction, $U_i = -2$ and no impurities ($w_i = 0$ for all sites on planes $\alpha < 1 - N_b/2$ and $\alpha > N_b/2$). We utilize the spinless Falicov–Kimball model to describe non-magnetic charge impurities within the barrier region. The interaction between dopant atoms and conduction electrons is attractive, and represented by a negative U_i^{FK}. The average impurity concentration within the barrier is given by $\rho_{imp} = (1/N_b)(a/L)^2 \sum w_i$, where $N_b(L/a)^2$ is the total number of atomic barrier sites (this model can be interpreted as an exactly solved annealed disorder problem, which does not describe weak localization effects, but does undergo a 'correlation-induced' metal–insulator transition at large enough U_{FK}). We also consider systems where there are no impurities within the barrier, but there is a Hubbard interaction for sites within the barrier, $U_i = U_b$, that differs from $U_i = -2$ in the superconductor (this system should be compared with the SS'S junctions of the analytic theories). In addition, we have included systems where the hopping integral, t_α, differs in the barrier region (to simulate Fermi-velocity mismatch), and where the interfacial planes ($\alpha = 1 - N_b/2$ and $\alpha = N_b/2$ only) have a non-zero local on-site potential, $\epsilon_\alpha = V_{Int}$ (to simulate SINIS or SISIS junctions).

We use the matrix formulation of Nambu [36] for the Green function, $\underline{\underline{G}}(r_i, r_j, i\omega_n)$, between two lattice sites r_i and r_j at the Matsubara frequency, $i\omega_n = i\pi(2n + 1)k_B T$,

$$\underline{\underline{G}}(r_i, r_j, i\omega_n) = \begin{pmatrix} G(r_i, r_j, i\omega_n) & F(r_i, r_j, i\omega_n) \\ \overline{F}(r_i, r_j, i\omega_n) & -G^*(r_i, r_j, i\omega_n) \end{pmatrix} \tag{2}$$

and the corresponding local self-energy,

$$\underline{\underline{\Sigma}}(r_i, i\omega_n) = \begin{pmatrix} \Sigma(r_i, i\omega_n) & \phi(r_i, i\omega_n) \\ \phi^*(r_i, i\omega_n) & -\Sigma^*(r_i, i\omega_n)) \end{pmatrix}. \tag{3}$$

The diagonal and off-diagonal Green functions are defined respectively as:

$$G(r_i, r_j, i\omega_n) = -\int_0^\beta d\tau \exp(i\omega_n \tau) \langle T_\tau \hat{c}_{j\sigma}(\tau) \hat{c}_{i\sigma}^\dagger(0) \rangle \tag{4}$$

$$F(r_i, r_j, i\omega_n) = -\int_0^\beta d\tau \exp(i\omega_n \tau) \langle T_\tau \hat{c}_{j\uparrow}(\tau) \hat{c}_{i\downarrow}(0) \rangle \tag{5}$$

where T_τ denotes time-ordering in τ and $\beta = 1/(k_B T)$.

The self energies and Green functions are coupled together through Dyson's equation,

$$\underline{\underline{G}}(r_i, r_j, i\omega_n) = \underline{\underline{G}}^{(0)}(r_i, r_j, i\omega_n) + \sum_l \underline{\underline{G}}^{(0)}(r_i, r_l, i\omega_n) \underline{\underline{\Sigma}}(r_l, i\omega_n) \underline{\underline{G}}(r_l, r_j, i\omega_n) \tag{6}$$

where we have included the local approximation for the self-energy, $\underline{\underline{\Sigma}}(r_i, r_j, i\omega_n) = \underline{\underline{\Sigma}}(r_i, i\omega_n)\delta_{ij}$, (which can be relaxed if we use the dynamical cluster approximation (DCA) [37, 38]). The non-interacting Green function, $\underline{\underline{G}}^{(0)}(r_i, r_j, i\omega_n)$ is diagonal in Nambu space, with upper diagonal component given by:

$$G^{(0)}(r_i, r_j, i\omega_n) = \int d^3k \frac{e^{ik \cdot (r_i - r_j)}}{i\omega_n - \varepsilon_k + \mu}. \tag{7}$$

We emphasize that $\underline{\underline{G}}^{(0)}$ is the non-interacting Green function and is *not* the effective medium of an equivalent atomic problem (see below for the detailed algorithm used to solve the dynamical mean field theory). A major innovation in our work is to utilize an efficient hybrid real-space–momentum-space method for calculating the Green functions from the set of local self-energies. We find this method to be much more powerful in solving systems with spatial variations or inhomogeneity, and it is also faster in bulk systems with current flow than a more conventional k-space integral technique.

Since the stacked planes have translational symmetry within the plane, the systems that we study are inhomogeneous in one direction only. We choose that direction to be labelled the z-axis, which is also the direction of current flow through the Josephson junction. The first stage of our method is to convert the problem from a three-dimensional system to a quasi-one-dimensional system following the algorithm of Potthoff and Nolting [31]. We perform a Fourier transform within the planes to determine the planar indexed Green functions,

$$\underline{\underline{G}}_{\alpha\beta}(i\omega_n, k_x, k_y) = \left(\frac{a}{L}\right)^2 \sum_{x_j, y_j} \underline{\underline{G}}(r_i, r_j, i\omega_n) \exp[ik_x(x_j - x_i) + ik_y(y_j - y_i)] \tag{8}$$

where α and β denote distinct planes, defined by $\alpha = z_i/a$, $\beta = z_j/a$ and the summation is over all lattice sites, (x_j, y_j), within the βth plane. The self-energy, $\underline{\underline{\Sigma}}_\alpha(i\omega_n) = \underline{\underline{\Sigma}}(z_i, i\omega_n) = \underline{\underline{\Sigma}}(r_i, i\omega_n)$, is independent of the planar coordinates x_i and y_i, so that Dyson's equation (equation (6)) becomes

$$\underline{\underline{G}}_{\alpha\beta}(i\omega_n, k_x, k_y) = \underline{\underline{G}}_{\alpha\beta}^{(0)}(i\omega_n, k_x, k_y) + \sum_\gamma \underline{\underline{G}}_{\alpha\gamma}^{(0)}(i\omega_n, k_x, k_y) \underline{\underline{\Sigma}}_\gamma(i\omega_n) \underline{\underline{G}}_{\gamma\beta}(i\omega_n, k_x, k_y) \tag{9}$$

with the summation over all planes, γ. The non-interacting planar Green function is similarly found by the Fourier transform

$$\underline{\underline{G}}^{(0)}_{\alpha\beta}(i\omega_n, k_x, k_y) = \left(\frac{a}{L}\right)^2 \sum_{x_j, y_j} \underline{\underline{G}}^{(0)}(\boldsymbol{r}_i, \boldsymbol{r}_j, i\omega_n) \exp[ik_x(x_j - x_i) + ik_y(y_j - y_i)]. \tag{10}$$

The local Green function, $\underline{G}(\boldsymbol{r}_i, \boldsymbol{r}_i, i\omega_n)$, is required for calculating the self-consistent potentials, and the Green function $\underline{G}(\boldsymbol{r}_i, \boldsymbol{r}_j, i\omega_n)$ between two neighbouring sites, $\boldsymbol{r}_i = (x_i, y_i, z_i)$ and $\boldsymbol{r}_j = (x_i, y_i, z_i \pm a)$ is required for current calculations. These are given by the simple planar momentum integrals:

$$\underline{G}(\boldsymbol{r}_i, \boldsymbol{r}_j, i\omega_n) = \left(\frac{\pi}{a}\right)^2 \int_{-\pi/a}^{\pi/a} \int_{-\pi/a}^{\pi/a} \underline{G}_{\alpha, \beta}(i\omega_n, k_x, k_y) dk_x\, dk_y \tag{11}$$

where again, $\alpha = z_i/a$ and $\beta = z_j/a$, and the phase factors in the integral have cancelled as $x_i = x_j$ and $y_i = y_j$. Hence our goal is to find the interacting Green functions, $\underline{\underline{G}}_{\alpha\beta}(i\omega_n, k_x, k_y)$.

We make a huge improvement (by one to two orders of magnitude) in the computational efficiency by transforming the two-dimensional planar momentum integral into a single integral over in-plane kinetic energy. In the case of nearest-neighbour hopping on a square lattice, the kinetic energy within the αth plane is given by

$$\varepsilon_\alpha^{xy} = -2t_\alpha[\cos(k_x a) + \cos(k_y a)] = \frac{t_\alpha}{t}\overline{\varepsilon^{xy}} \tag{12}$$

where t_α is the hopping integral between two nearest-neighbour sites within the αth plane and a is the lattice spacing. The effect of the in-plane kinetic energy is equivalent to an increase in the on-site energy, $\epsilon_i^{(0)} \mapsto \epsilon_i^{(0)} + \varepsilon_\alpha^{(xy)}$ which can vary between the different planes. The planar Green functions only depend on the planar momentum via the normalized kinetic energy, $\overline{\varepsilon^{xy}} = -2t[\cos(k_x a) + \cos(k_y a)]$, such that $\underline{\underline{G}}_{\alpha\beta}(i\omega_n, k_x, k_y) = \underline{\underline{G}}_{\alpha\beta}(i\omega_n, \overline{\varepsilon^{xy}})$. Hence, by using the two-dimensional density of states, $\rho^{2D}(\varepsilon)$, for a square lattice, the momentum integral is transformed into

$$\left(\frac{a}{2\pi}\right)^2 \int_{-\pi/a}^{\pi/a} \int_{-\pi/a}^{\pi/a} G_{\alpha\beta}(i\omega_n, k_x, k_y)\, dk_x\, dk_y = \int_{-\infty}^{\infty} G_{\alpha\beta}(i\omega_n, \overline{\varepsilon^{xy}})\rho^{2D}(\overline{\varepsilon^{xy}})\, d\overline{\varepsilon^{xy}}. \tag{13}$$

The specific hopping integral, t_α, for each plane affects the on-site potential of a given plane in the continued-fraction method (see equation (15) below), but does not contribute to the change of variables in the momentum integral.

Once the system is converted to a quasi-one-dimensional model, with nearest-neighbour hopping, the Green functions can be solved rapidly by a continued-fraction expansion, without recourse to another k-space integral for the z-direction. The continued-fraction expansion is similar to the recursion method [39, 40], modified to include superconductivity [41], but with three important differences. First, the method is much faster, as there is no need to expand about a site to obtain a new basis—the system is already one dimensional in form. Second, there is no inaccuracy in the termination process, as the hopping integrals are given exactly in the model. The third point is an alteration, because the sites of interest are not at the end of a chain, but in the middle. This leads to a different set of continued fractions that must be calculated compared with the standard recursion method. In test runs, our method proves to be 4×10^5 times faster, and with machine precision accuracy, compared to a standard recursion method expansion which is terminated (due to memory limits) at an accuracy of one part in 10^3! An alternate approach is to solve Dyson's matrix equation directly for a finite system, where the infinitely extended bulk boundaries can be mimicked by appropriate choice of potentials

for the end planes. We have carried out such an approach as a comparison, but find it to be much slower (by a factor of 4000 for 60 planes than our method, and it grows like N^3 for large systems with N planes) so we only describe the continued-fraction method below.

The equivalence of our method to the recursion method is that we calculate the Green functions directly from a continued-fraction representation of the inverse of the Hamiltonian matrix in real space. That is, we find

$$
\underline{\underline{G}}_{\alpha\beta}(i\omega_n, \overline{\varepsilon^{xy}}) = \begin{pmatrix} \ddots & \ddots & 0 & \vdots & \vdots & \vdots & \\ \ddots & i\omega_n\underline{\underline{1}} - \underline{\underline{a}}_{\alpha-2} & \underline{\underline{b}}_{\alpha-1} & 0 & 0 & 0 & \cdots \\ \cdots & \underline{\underline{b}}^\dagger_{\alpha-1} & i\omega_n\underline{\underline{1}} - \underline{\underline{a}}_{\alpha-1} & \underline{\underline{b}}_{\alpha} & 0 & 0 & \cdots \\ \cdots & 0 & \underline{\underline{b}}^\dagger_{\alpha} & i\omega_n\underline{\underline{1}} - \underline{\underline{a}}_{\alpha} & & & \\ \cdots & 0 & 0 & \underline{\underline{b}}^\dagger_{\alpha+1} & i\omega_n\underline{\underline{1}} - \underline{\underline{a}}_{\alpha+1} & \underline{\underline{b}}_{\alpha+2} & 0 \\ & \vdots & \vdots & 0 & \ddots & \ddots & \ddots \end{pmatrix}^{-1}_{\alpha\beta}
$$

(14)

where the matrices $\{\underline{\underline{a}}_\alpha\}$ are the total in-plane energies for a particular plane, given by

$$
\underline{\underline{a}}_\alpha = \begin{pmatrix} \epsilon_\alpha + \varepsilon^{(xy)}_\alpha + \Sigma_\alpha(i\omega_n) - \mu & \phi_\alpha(i\omega_n) \\ \phi^*_\alpha(i\omega_n) & -\epsilon_\alpha - \varepsilon^{(xy)}_\alpha - \Sigma^*_\alpha(i\omega_n) + \mu \end{pmatrix}
$$

(15)

and $\{\underline{\underline{b}}_\alpha\}$ couple the $(\alpha-1)$th and αth planes,

$$
\underline{\underline{b}}_\alpha = \begin{pmatrix} -t_{\alpha-1,\alpha} & 0 \\ 0 & t^*_{\alpha-1,\alpha} \end{pmatrix}.
$$

(16)

The local planar Green function, $\underline{\underline{G}}_{\alpha\alpha}(i\omega_n, \overline{\varepsilon^{xy}})$, is readily evaluated as a combination of continued fractions (as in the renormalized perturbation expansion [42]). We define the right-directed, $\underline{\underline{R}}_\alpha(i\omega_n)$, and left-directed $\underline{\underline{L}}_\alpha(i\omega_n)$ continued fractions from a plane, α, recursively as

$$
\underline{\underline{R}}_\alpha(i\omega_n, \overline{\varepsilon^{xy}}) = i\omega_n\underline{\underline{1}} - \underline{\underline{a}}_\alpha - \underline{\underline{b}}_{\alpha+1}\underline{\underline{R}}^{-1}_{\alpha+1}(i\omega_n, \overline{\varepsilon^{xy}})\underline{\underline{b}}^\dagger_{\alpha+1}
$$

(17)

$$
\underline{\underline{L}}_\alpha(i\omega_n, \overline{\varepsilon^{xy}}) = i\omega_n\underline{\underline{1}} - \underline{\underline{a}}_\alpha - \underline{\underline{b}}^\dagger_\alpha\underline{\underline{L}}^{-1}_{\alpha-1}(i\omega_n, \overline{\varepsilon^{xy}})\underline{\underline{b}}_\alpha .
$$

(18)

The recursive calculation continues to infinity, but once it has been extended to planes in the uniform bulk medium, where $\alpha < 1 - N/2$ or $\alpha > N/2$, the coefficients at each level become constant. The effect of a constant phase gradient in ϕ is equivalent to a constant phase factor in the hopping integral, $t_{\alpha,\alpha+1}$, that does not change between planes in the bulk. Hence, by equating all $\underline{\underline{R}}_\alpha(i\omega_n, \overline{\varepsilon^{xy}})$ as $\underline{\underline{R}}_\infty(i\omega_n, \overline{\varepsilon^{xy}})$ for $\alpha > N/2$ and $\underline{\underline{L}}_\alpha(i\omega_n, \overline{\varepsilon^{xy}})$ as $\underline{\underline{L}}_\infty(i\omega_n, \overline{\varepsilon^{xy}})$ for $\alpha < 1 - N/2$ in the bulk limit, an exact terminator function can be calculated as the solution of a complex quadratic matrix equation:

$$
\underline{\underline{R}}_\infty(i\omega_n, \overline{\varepsilon^{xy}})\underline{\underline{b}}^{\dagger-1}_\infty\underline{\underline{R}}_\infty(i\omega_n, \overline{\varepsilon^{xy}}) + [\underline{\underline{a}}_\infty - i\omega_n\underline{\underline{1}}]\underline{\underline{b}}^{\dagger-1}_\infty\underline{\underline{R}}_\infty(i\omega_n, \overline{\varepsilon^{xy}}) + \underline{\underline{b}}_\infty = \underline{\underline{0}}
$$

(19)

$$
\underline{\underline{L}}_\infty(i\omega_n, \overline{\varepsilon^{xy}})\underline{\underline{b}}^{-1}_\infty\underline{\underline{L}}_\infty(i\omega_n, \overline{\varepsilon^{xy}}) + [\underline{\underline{a}}_\infty - i\omega_n\underline{\underline{1}}]\underline{\underline{b}}^{-1}_\infty\underline{\underline{L}}_\infty(i\omega_n, \overline{\varepsilon^{xy}}) + \underline{\underline{b}}^\dagger_\infty = \underline{\underline{0}}.
$$

(20)

Note that the same terminator function is used for all sites in the intermediate layers, and the functions $\underline{\underline{R}}_\alpha$ and $\underline{\underline{L}}_\alpha$ calculated for one site are used in the calculation for the next site—so the number of computations required to find solutions for all sites can be O(N).

There are two ways to solve this matrix quadratic equation. When we perform calculations on the real axis, without including a supercurrent, the matrix equation becomes analytically tractable to solve. On the imaginary axis, we find that it is numerically faster to simply use

an iterative solution to these quadratic equations within the bulk medium. In most cases, accuracies of one part in 10^{10} can be achieved in ten iterations or less.

The continued fractions form the local planar Green functions, according to

$$\underline{\underline{G}}_{\alpha\alpha}(\mathrm{i}\omega_n, \overline{\varepsilon^{xy}}) = \{\mathrm{i}\omega_n\underline{\underline{1}} - \underline{\underline{a}}_\alpha(\overline{\varepsilon^{xy}}) - \underline{\underline{b}}^\dagger_\alpha\underline{\underline{L}}^{-1}_{\alpha-1}(\mathrm{i}\omega_n, \overline{\varepsilon^{xy}})\underline{\underline{b}}_\alpha - \underline{\underline{b}}_{\alpha+1}\underline{\underline{R}}^{-1}_{\alpha+1}(\mathrm{i}\omega_n, \overline{\varepsilon^{xy}})\underline{\underline{b}}^\dagger_{\alpha+1}\}^{-1} \quad (21)$$

which, using equations (17) and (18), can be simplified to

$$\underline{\underline{G}}_{\alpha\alpha}(\mathrm{i}\omega_n, \overline{\varepsilon^{xy}}) = [\underline{\underline{R}}_\alpha + \underline{\underline{L}}_\alpha - \mathrm{i}\omega_n\underline{\underline{1}} + \underline{\underline{a}}_\alpha]^{-1}. \quad (22)$$

The Green functions connecting neighbouring planes, α and $\alpha \pm 1$, which are required to calculate the current flow, are given in two equivalent forms

$$\underline{\underline{G}}_{\alpha,\alpha+1}(\mathrm{i}\omega_n, \overline{\varepsilon^{xy}}) = -\underline{\underline{G}}_{\alpha\alpha}(\mathrm{i}\omega_n, \overline{\varepsilon^{xy}})\underline{\underline{b}}_{\alpha+1}\underline{\underline{R}}^{-1}_{\alpha+1}(\mathrm{i}\omega_n, \overline{\varepsilon^{xy}})$$
$$= -\underline{\underline{L}}^{-1}_\alpha(\mathrm{i}\omega_n, \overline{\varepsilon^{xy}})\underline{\underline{b}}_{\alpha+1}\underline{\underline{G}}_{\alpha+1,\alpha+1}(\mathrm{i}\omega_n, \overline{\varepsilon^{xy}}) \quad (23)$$

$$\underline{\underline{G}}_{\alpha,\alpha-1}(\mathrm{i}\omega_n, \overline{\varepsilon^{xy}}) = -\underline{\underline{G}}_{\alpha\alpha}(\mathrm{i}\omega_n, \overline{\varepsilon^{xy}})\underline{\underline{b}}^\dagger_\alpha\underline{\underline{L}}^{-1}_{\alpha-1}(\mathrm{i}\omega_n, \overline{\varepsilon^{xy}})$$
$$= -\underline{\underline{R}}^{-1}_{\alpha+1}(\mathrm{i}\omega_n, \overline{\varepsilon^{xy}})\underline{\underline{b}}^\dagger_\alpha\underline{\underline{G}}_{\alpha-1,\alpha-1}(\mathrm{i}\omega_n, \overline{\varepsilon^{xy}}). \quad (24)$$

The local planar Green functions enable us to calculate the self-energy and electron density, n_i, on each site in a given plane, $\alpha = z_i/a$, with the latter given by

$$n_i = k_B T \sum_{\omega_n} \int_{-\infty}^{\infty} \rho^{2D}(\overline{\varepsilon^{xy}})\mathrm{Im}\,[G_{\alpha\alpha}(\mathrm{i}\omega_n, \overline{\varepsilon^{xy}})]\,\mathrm{d}\overline{\varepsilon^{xy}}. \quad (25)$$

The current, $I_{\alpha,\alpha+1}$, which flows along each link between two neighbouring planes, α and $\alpha+1$, in the z-direction is given by

$$I_{\alpha,\alpha+1} = \frac{2eat}{\hbar}k_B T \sum_{\omega_n} \int_{-\infty}^{\infty} \rho^{2D}(\overline{\varepsilon^{xy}})\mathrm{Im}\,[G_{\alpha,\alpha+1}(\mathrm{i}\omega_n, \overline{\varepsilon^{xy}})]\,\mathrm{d}\overline{\varepsilon^{xy}} \quad (26)$$

(note this is a current per unit cell, equal to a current density times the unit cell area, a^2). A stringent convergence check for self-consistency, when there is a phase difference between the bulk superconductors, is that the current flow is constant from one plane to the next. Note that our self-consistent solutions are *fully* self-consistent in that both the phase and magnitude of the gap are determined self-consistently and we do not average over short distances, so we can see effects due to oscillations on the scale of the inverse Fermi wavelength. Self-consistency has only been included in a small subset of all calculations on Josephson junctions [43] but it becomes increasingly important for short-coherence-length superconductors [35].

For the bulk boundary regions, the uniform variation of phase in the off-diagonal self-energy, $\phi(\boldsymbol{r}_i)$ has the form $\phi(\boldsymbol{r}_i) = \phi_0 \exp[\mathrm{i}\boldsymbol{q}\cdot\boldsymbol{r}_i]$, where the net superfluid momentum depends on $\boldsymbol{q} = (0, 0, q_z)$ through $mv_s = (\hbar/a)\sin(q_z a)$ and leads to the following solution of Dyson's equation:

$$G(\boldsymbol{r}_i, \boldsymbol{r}_j, \mathrm{i}\omega_n) = \int \mathrm{d}^3k \frac{(\mathrm{i}\omega_n + \varepsilon_{k-q} - \mu + \Sigma^*(\mathrm{i}\omega_n))\,\mathrm{e}^{\mathrm{i}\boldsymbol{k}\cdot(\boldsymbol{r}_i-\boldsymbol{r}_j)}}{(\mathrm{i}\omega_n - \varepsilon_k + \mu - \Sigma(\mathrm{i}\omega_n))(\mathrm{i}\omega_n + \varepsilon_{k-q} - \mu + \Sigma^*(\mathrm{i}\omega_n)) - |\phi_0(\mathrm{i}\omega_n)|^2} \quad (27)$$

and

$$F(\boldsymbol{r}_i, \boldsymbol{r}_j, \mathrm{i}\omega_n) = \int \mathrm{d}^3k \frac{\phi_0(\mathrm{i}\omega_n)\mathrm{e}^{\mathrm{i}(\boldsymbol{k}-\boldsymbol{q})\cdot(\boldsymbol{r}_i-\boldsymbol{r}_j)}}{(\mathrm{i}\omega_n - \varepsilon_k + \mu - \Sigma(\mathrm{i}\omega_n))(\mathrm{i}\omega_n + \varepsilon_{k-q} - \mu + \Sigma^*(\mathrm{i}\omega_n)) - |\phi_0(\mathrm{i}\omega_n)|^2} \quad (28)$$

where the diagonal self-energy, $\Sigma(\mathrm{i}\omega_n)$, is independent of site index, $\boldsymbol{r}_i$, in the bulk. We will need only the local, and nearest-neighbour bulk Green functions in our calculations.

The superconducting region is modelled by the negative-U Hubbard model within the Hartree–Fock (static mean-field) approximation (this approach is identical to BCS theory except the low-energy cutoff is provided by the electronic bandwidth rather than the phonon frequency [35]). In this case, the local self-energy is found from the local Green functions by

$$\Sigma(r_i, i\omega_n) = UT \sum_{\omega_n} G(r_i, r_i, i\omega_n) \tag{29}$$

and

$$\phi(r_i, i\omega_n) = -UT \sum_{\omega_n} F(r_i, r_i, i\omega_n) \tag{30}$$

where the instantaneous electron–electron interaction energy, U, leads to a time-independent self-energy. This procedure is identical to the conventional Bogoliubov–de Gennes approach [44], which neglects retardation effects in the superconductor (it also can be viewed as solving a lattice version of the Eilenberger equations which are evaluated for an arbitrary and self-consistently determined relaxation length within the barrier). As all sites within a plane are identical, the self-energy need only be calculated once for each of the N planes.

For planes within the barrier which include impurities, the dynamical mean field approximation says that the local (site) Green function, $\underline{\underline{G}}(r_i, r_i, i\omega_n)$ is related to a local host Green function [45], $\underline{\underline{\mathcal{G}}}(r_i, i\omega_n)$, via

$$\underline{\underline{\mathcal{G}}}(r_i, i\omega_n) = [\underline{\underline{G}}^{-1}(r_i, r_i, i\omega_n) + \underline{\underline{\Sigma}}(r_i, i\omega_n)]^{-1}. \tag{31}$$

The atomic Green function, $\underline{\underline{G}}^{at}(r_i, i\omega_n)$, which will be equated to the local Green function, $\underline{\underline{G}}(r_i, r_i, i\omega_n)$, in the dynamical mean field approximation, then satisfies

$$\underline{\underline{G}}^{at}(r_i, i\omega_n) = (1 - \rho_{imp})\underline{\underline{\mathcal{G}}}(r_i, i\omega_n) + \rho_{imp}[\underline{\underline{\mathcal{G}}}^{-1}(r_i, i\omega_n) - U^{FK}\underline{\underline{1}}]^{-1}. \tag{32}$$
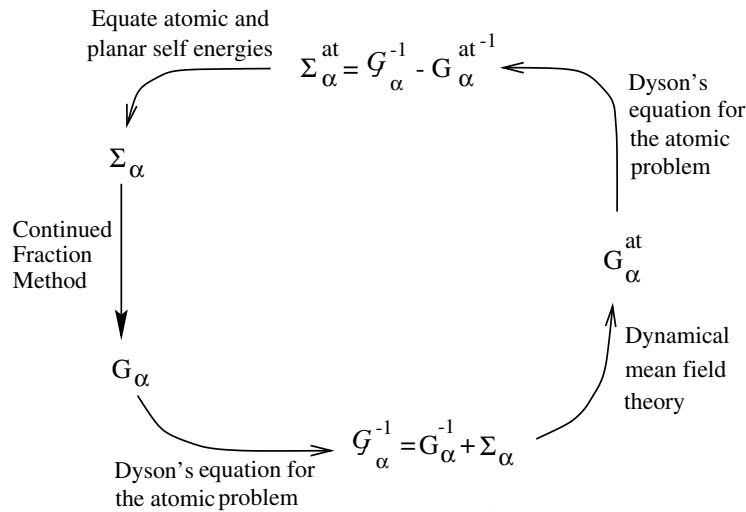
and the local self-energy becomes

$$\underline{\underline{\Sigma}}(r_i, i\omega_n) = \underline{\underline{\mathcal{G}}}^{-1}(r_i, i\omega_n) - \underline{\underline{G}}^{at\,-1}(r_i, i\omega_n). \tag{33}$$

Starting from a local self-energy, $\underline{\underline{\Sigma}}(r_i, i\omega_n)$, and a local Green function, $\underline{\underline{G}}(r_i, r_i, i\omega_n)$, equations (31)–(33) can be employed to iteratively determine a new self-energy $\underline{\underline{\Sigma}}(r_i, i\omega_n)$ when the plane is described by the Falicov–Kimball model. The method, which is solved for a fixed concentration of impurities, ρ_{imp}, is equivalent to the coherent potential approximation and solves exactly for the dynamical effects of annealed charge impurities. The algorithm is summarized in figure 2. Note that this treatment of impurity scattering goes beyond assuming an energy independent relaxation time, as is usually done in analytic approaches, but rather includes all correlation effects and interpolates smoothly through the quantum critical point of the metal–insulator transition.

3. Phase variation

Standard theory of Josephson junctions [1] predicts the phase variation of the current in the weak-coupling limit to be $I(\theta) = I_c \sin(\theta)$ where θ is the phase difference across the barrier, and I_c is the temperature-dependent critical current. Such a current variation arises from consideration of two superconductors with different phases being coupled by a single energy-independent transmission coefficient, corresponding to the tunnelling of Cooper pairs across a barrier. A more general consideration [24] includes the Bogoliubov–de Gennes equations for a one-dimensional system of two superconductors coupled across a potential barrier, V. The strength of the barrier is measured by $Z = mV/\hbar^2 k_F$ which

Equate atomic and
planar self energies

$$\Sigma_\alpha^{at} = \mathcal{G}_\alpha^{-1} - G_\alpha^{at\,-1}$$

Dyson's
equation for
the atomic
problem

Σ_α

Continued
Fraction
Method

G_α^{at}

Dynamical
mean field
theory

G_α

$$\mathcal{G}_\alpha^{-1} = G_\alpha^{-1} + \Sigma_\alpha$$

Dyson's equation for
the atomic problem

Figure 2. Diagram of the iteration procedure, where the dynamical mean field theory is used to calculate local self-energies from local Green functions. In the case of the Hartree–Fock approximation for the self-energy, the dynamical mean field theory step is trivial (see equations (29)–(30)).

determines the transmission coefficient, τ, according to $\tau = 1/(1 + Z^2)$. It is found that Andreev bound states carry the current, whose maximum as a function of θ increases from $\pi/2$ towards π with increasing transmission coefficient [21–25]. In all such cases, of both one- and three-dimensional geometry, it is seen that the linear response current, $I' = (\mathrm{d}I/\mathrm{d}\theta)_{\lim \theta \mapsto 0}$ is proportional to the normal state conductance. This results in the product $I'R_N = (\pi \Delta_0(T)/2e) \tanh(\Delta_0(T)/2k_B T)$ being independent of the microscopic details of the barrier. We will show that a self-consistent, microscopic treatment for barrier lengths on the order of the coherence length results in variations of $I'R_N$.

Further differences arise between methods which treat the barrier as a single scattering potential and our self-consistent treatment of the order parameter and off-diagonal Green functions within the barrier. Our results indicate that the effective scattering strength of the barrier, Z, increases with temperature and current flow. In general, the proximity effect, which enhances coupling between superconductors, is weakened as the current flow approaches the critical current. Hence at large current flow, the effective barrier is increased compared to its value in the linear response regime at close to zero current flow. The effect of self-consistency on the current–phase relationship appears to be more marked for thin barriers, where the current flow becomes relatively large.

We quantify the current response by making use of the linear response, I', as well as the maximum current flow, I_c, through the barrier. In the weak-coupling limit, I_c is exactly equal to I', and our results show that in general the two are within 20% of each other and scale almost identically with external parameters. As I' requires much less computational time to calculate, than I_c, we report values of I' for many of our results.

4. Bogoliubov–de Gennes results

To begin, we demonstrate how our model reproduces standard results, by using the Hartree–Fock approximation to calculate the self-energy within the barrier region. As such, we

are essentially self-consistently solving the full three-dimensional Bogoliubov–de Gennes equations (or equivalently, a lattice version of the Eilenberger equations) for the system. Nevertheless, we find that self-consistency produces a number of novel results. In all the results that we present in this paper, the superconducting region is modelled with an attractive Hubbard interaction of $U = -2$ at half filling. The homogeneous bulk superconductor then has a critical temperature $T_c = 0.11$ and a zero-temperature order parameter $\Delta_0 = 0.198$. The coherence length $\xi = \hbar v_f/(\pi \Delta)$ can be estimated to range from $3.5a$ to $4.3a$ depending on whether we choose to average the absolute value of v_f over the Fermi surface or to take the root mean square of v_f over the Fermi surface.
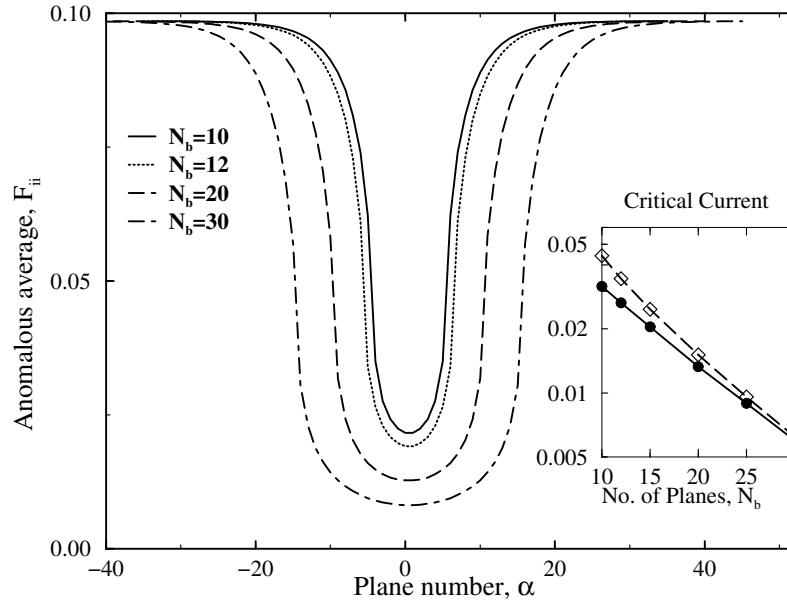
Figure 3. Plot of the decay of the anomalous average due to the proximity effect in the barrier region. Note that the order parameter, Δ is equal to $2F_{ii} = 2F(r_i, r_i, \tau = 0^+)$ in the superconducting region, where $U = -2$, and is equal to $F_{ii}/2$ in the barrier region, as $U_b = -1/2$. It is the anomalous Green function, F_{ii}, rather than the order parameter, Δ_i, that is continuous throughout the system. The inset figure shows the exponential decay of the linear response current, I' (upper, dashed curve), and critical current, I_c (lower, solid curve), with increasing barrier thickness. Note how both I' and I_c systematically track with each other, and agree to within 20% for cases considered here. (The current units are per unit square $4et/(ha^2)$.)

We begin by solving for systems with a small attractive interaction within the barrier, $U_b = -0.5$, over a range of barrier thicknesses. This attraction is small enough that the bulk superconducting transition temperature of the barrier material is always less than any temperature we consider. Figure 3 demonstrates the proximity effect, with the decay of the anomalous average at the centre of the barrier as its thickness is increased. A fit of the decay into the superconductor gives an exponential behaviour with a coherence length of approximately $3.7a$, which agrees with our bulk estimate above. Inset is a log plot of the linear-response current and critical current against barrier thickness. As expected, both the linear-response current, I', and the critical current, I_c, drop rapidly when the number of planes within the barrier region is increased from five to 30. The nearly constant slopes indicate that the decays are close to exponential. The exponent (which determines the coherence length within the barrier) is $13.3a$, which is approximately three to four times the bulk coherence length. More importantly,
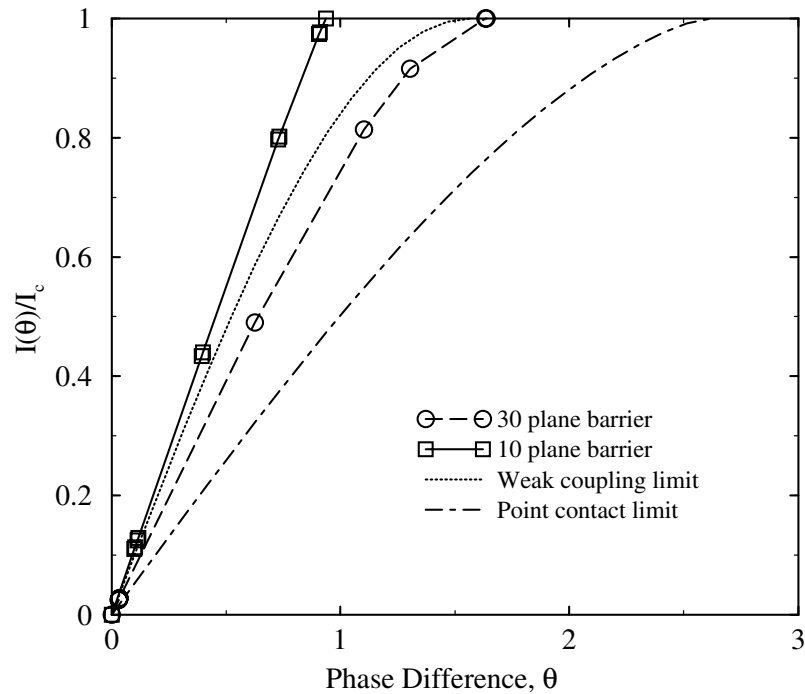
Figure 4. Current flow as a function of phase difference across the barrier for a thin and a thick junction, compared to analytic results for a low-transparency (dotted curve) and a high-transparency (chain-dashed cruve) junction. Notice how the results for a thin junction lie outside of the results for the two analytic limiting cases. This shows how including self-consistency and a microscopic model of the barrier thickness can affect the current–phase relation.

the inset shows how I_c and I' track with each other for a variety of barrier thicknesses. Note that this nearly pure exponential decay of I_c with barrier thickness d differs from the analytic prediction [11] which would say that $I_c = ad/\xi \exp(-d/\xi)$ for some constant a. The data fit much better to a functional form that does not have the d/ξ prefactor. We believe this difference arises from the self-consistency in the intermediate-barrier-length regime.

Figure 4 shows the normalized current as a function of phase difference across the barrier region, for two different barrier thicknesses. The phase variation is compared to the simple form $I(\theta)/I_c = \sin(\theta)$, which is appropriate in the weak-coupling limit [21], and $I(\theta)/I_c = (I_0/I_c)\sin(\theta/2)\tanh(\Delta\cos(\theta/2)/2k_BT)$, the result for a point-contact junction [22], appropriate in the limit of high transparency. The curve for a thin junction falls outside these two limits, indicating that the effects of self-consistency and finite junction thickness are important in determining the current–phase relation for these Josephson junctions [26]. In particular, the calculated difference between a weakly coupled and strongly coupled junction lies in the opposite direction to the analytic formula on such a normalized curve. The actual magnitude of the critical current, is of course, greatly enhanced for the thinner barrier, as shown in the inset to figure 3.

Figure 5 demonstrates the proximity effect as a decay in the anomalous average, $F_{ii} = F(\mathbf{r}_i, \mathbf{r}_i, \tau = 0^+)$, within a barrier region of 20 planes. The proximity effect is seen to depend on the Hubbard interaction, U_b, for sites within the barrier. The corresponding critical currents, I_c and linear response currents, I', are shown inset in figure 5. Note that in
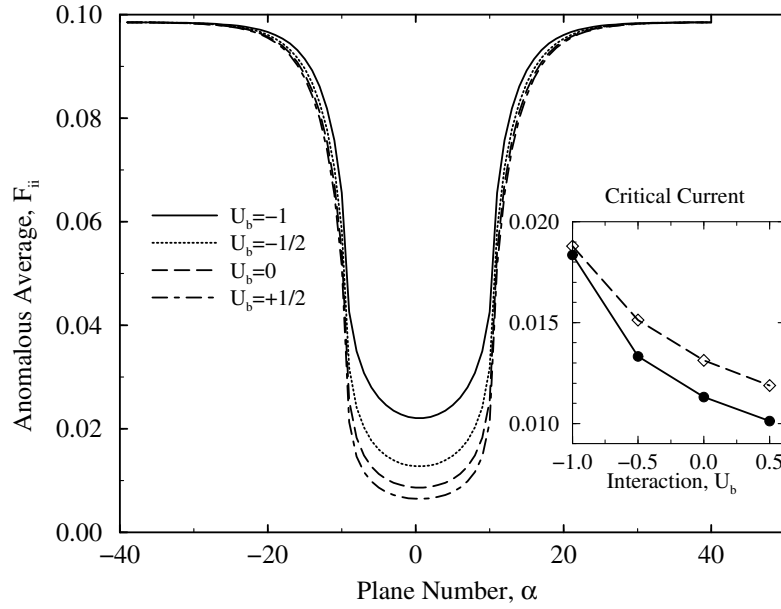
Figure 5. Decay of the anomalous average within the barrier region as a function of the Hubbard interaction, U_b. The anomalous average decays more rapidly as the Coulomb interaction in the barrier, U_b, increases in value (and becomes repulsive). The inset figure depicts the linear response current, I' (upper, dashed curve), and critical current, I_c (lower solid curve), as a function of U_b. Note how both critical currents fall with U_b, and note that there is no apparent discontinuity through $U_b = 0$, where the sign of Δ changes within the barrier.

the cases where U_b is negative, the barrier region is actually a superconductor in its normal state, above its transition temperature. In the case where $U_b = 0$, the order parameter, Δ_i, is exactly zero within the barrier. In the example where U_b is positive, the order parameter actually switches sign within the barrier region, even when there is no external phase variation. The results of the inset figure indicate that such a switching in sign of the pairing potential, Δ_i has no marked effect on the transport properties, which depend on the continuously varying Green functions of the system. Once again we find a systematic tracking of I' and I_c with the strength of the Coulomb interaction, U_b, in the barrier.

Our method allows us to consider different hopping integrals in different regions (within planes or between planes). This would be appropriate when the barrier region has a density of states at the Fermi surface (or a Fermi velocity) that differs from that found in the normal state of the superconducting regions. When modelling such systems, the hopping integral between successive planes that have differing intraplanar hopping integrals, is taken as the geometric mean of the two planar values ($t_{\alpha,\alpha+1} = \sqrt{t_\alpha t_{\alpha+1}}$).

The proximity effect results in a minimum of the anomalous average, $F_{ii} = F(\mathbf{r}_i, \mathbf{r}_i, \tau = 0^+) = \langle c_{i\uparrow}(0^+)c_{i\downarrow}(0)\rangle$, at the centre of the barrier region. At low temperatures, Figure 6(a) indicates that the system with a smaller hopping integral in the barrier, $t_b = 1/2$, has a larger anomalous average than the uniform system (with $t_b = 1$), due to its increase in density of states at the Fermi surface. As the temperature is increased, there is a crossover, with the system that has the largest hopping integral in the barrier ($t_b = 2$) having the largest anomalous average just below the critical temperature, T_c. Such a crossover is due to the differing natural energy scales, t_b, in the barrier region. For the system with $t_b = 1/2$, an actual temperature
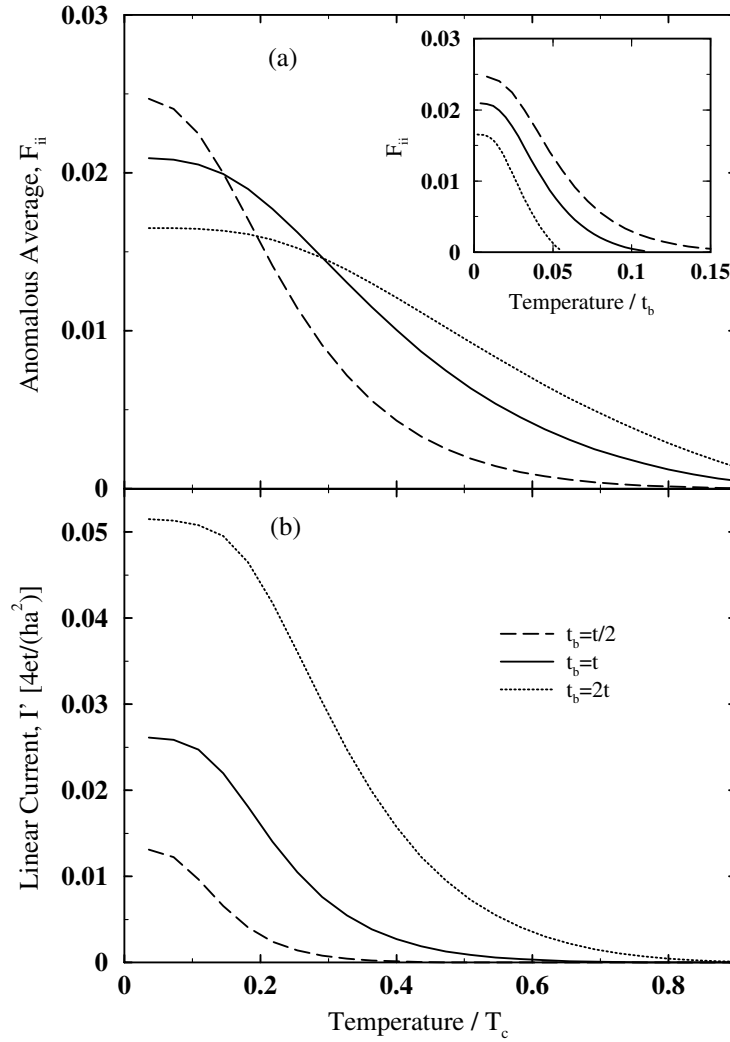
Figure 6. (a) Variation with temperature of the anomalous average, $F_{ii} = F(r_i, r_i, \tau = 0^+)$, for the plane at the centre of the barrier region. The different curves are results for different values of the barrier hopping integral, t_b. The inset figure depicts the scaling of the curves, when the temperature is normalized by the hopping integral, t_b. (b) Linear current, I', versus temperature for barriers with a hopping integral, t_b, that can differ from the hopping integral, t, between planes of the superconductor. Note how I' increases with t_b in the low-temperature regime.

of $T = 0.1$ corresponds to a temperature of 0.2 in the natural energy units of the barrier, t_b. When the temperatures are given in units of t_b, as shown inset in figure 6(a), a series of approximately parallel curves is seen, ordered according to the differing densities of states at the Fermi surface. The anomalous average, F_{ii}, plotted on the y-axis, does not require such scaling, as it is dimensionless.

Figure 6(b) indicates that the critical current approximately scales with the hopping integral in the barrier region at low temperature. This effect dominates over any increased scattering at the interfaces due to Fermi velocity mismatch. In fact, when t_b is large, the critical current is enhanced by a factor of t_b/t over that found in the uniform bulk system ($t_b = 1$).
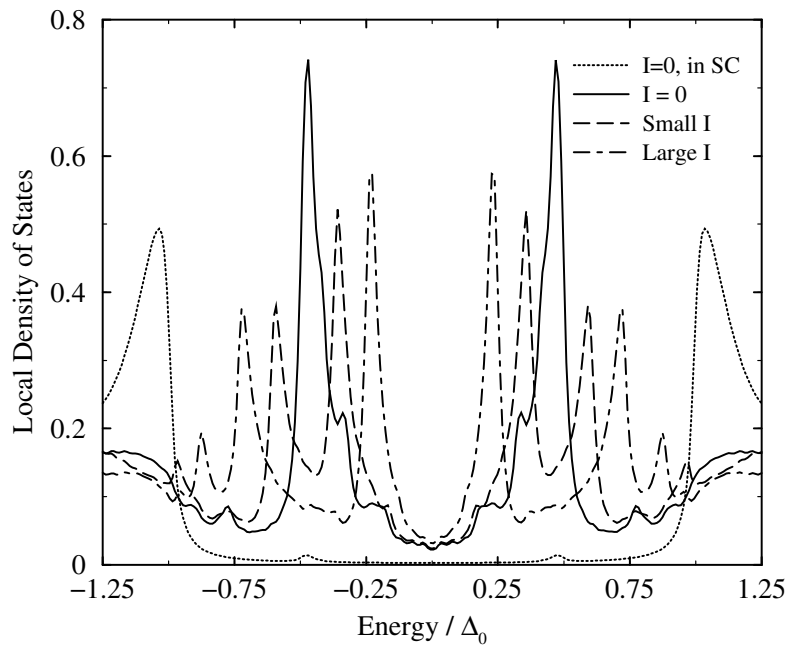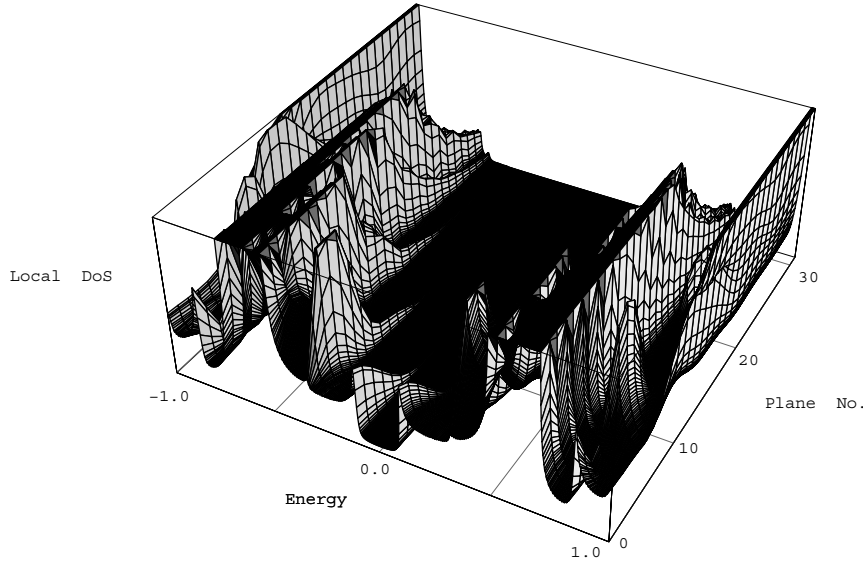
Figure 7. Local density of states at the centre of a Josephson junction (the plane $\alpha = 0$), with increasing current flow through the device ($N_b = 20$). The solid line is for zero current, the dashed curve is for small current, and the chain-dashed curve is for large current. The density of states within the superconducting region (plane $\alpha = 25$) at zero current flow, where $\Delta_0 = 0.198$ is shown in the dotted curve as a comparison. Note that the small bump at $E = 0.5\Delta_0$ for the superconducting region arises from the self-consistency relation and the proximity of this superconducting plane to the barrier. An imaginary part equal to 0.005 was added to the self-energy to smooth the density of states; this artificially produces a nonzero density of states at zero energy.

It is interesting to observe the density of states, in particular the presence of states within the gap as shown in figure 7. The two major peaks correspond to Andreev bound states, which carry current, when there is a phase difference across the barrier region. The bound states can be seen to split in two, so that two inner peaks move towards each other, while two outer peaks move to the gap edge as the current flow increases. This is an example of the Doppler shift for Andreev states bound within a barrier in a s-wave Josephson junction. An equivalent Doppler shift has been seen experimentally by tunnelling into the surface states that give rise to the zero-bias conductance peak in d-wave superconductors [46, 47].

A careful examination of the curve corresponding to zero current reveals a great deal of structure, due to states trapped within the barrier region (which is not represented well by a simple Lorentzian line shape). The exact energies of the bound states depend on the thickness of the barrier, and the states arise in part from normal reflection of quasiparticles with non-zero momenta parallel to the planes [48–50]. The intraplanar momenta of the quasiparticles may lead to the states being unobservable as current peaks at the corresponding voltages in an I–V curve, where only quasiparticles travelling perpendicular to the planes are measured. In figure 8, we examine the bound states in more detail, for a system with ten barrier planes ($N_b = 10$). It is worthwhile noting that as the energy of the states within the gap approaches the gap edge, so they extend further away from the barrier, into the superconducting region (which begins after the fifth plane from the centre ($\alpha > 5$)). The figure also demonstrates an alternating parity between states. The states with energy closest to zero have even parity,

Figure 8. The evolution of the local density of states within the gap, as a function of position in a Josephson junction. The energy axis is normalized by $\Delta_0 = 0.198$. Note there are even parity bound states, with a maximum at the centre plane, and odd parity states with a node at that point. The self-consistent solution is for a barrier of thickness ten planes ($N_b = 10$).

as demonstrated by a maximum amplitude at the central planes ($\alpha = 0, 1$). The next higher energy bound states have a node at the central planes, so exhibit odd parity.

We can define a current-carrying local density of states such that the total current per unit cell area a^2, $I_{\alpha,\alpha+1}$, between two successive planes, α and $\alpha + 1$, is given by

$$I_{\alpha,\alpha+1} = \int i_{\alpha,\alpha+1}(E)\,\mathrm{d}E. \tag{34}$$

A plot of the function $i_{\alpha,\alpha+1}(E)$ between the two planes, $\alpha = 0$ and $\alpha + 1 = 1$, at the centre of the barrier is shown in figure 9. It can be seen that the majority of the current is carried by the Andreev bound states, and that the two peaks that have separated from a single Andreev peak at zero phase difference, carry current in opposite directions. The states at positive energy carry equal and opposite current to the states at negative energy, but their occupation is much lower for low temperatures, $T \ll T_c$.

By including an extra repulsive or attractive potential on the interfacial planes which connect the barrier to the superconductor, we are able to model in a very simple manner, some of the effects of a charge accumulation region or a Schottky barrier (corresponding to an SINIS junction). In our simple model there is particle–hole symmetry for a half-filled band: a repulsive potential depletes the electron density in one layer, to reproduce some effects of a Schottky barrier, while an attractive potential results in a charge accumulation region. The effect on the pairing potential and current density are the same, for equivalent potential strengths at half-filling. That is, if a repulsive interfacial potential, V_1, results in a reduction in electron density on a specific plane, then the attractive potential, $-V_1$, at the interface, causes an equal in magnitude increase of electron density at that plane, and results in a system with the same variation in order parameter, and equal current response.

Figure 10(a) indicates the oscillations in the anomalous average resulting from a single layer barrier with $V_0 = \pm 2t$ and $V_0 = \pm 4t$. Notice that the proximity effect is reduced by
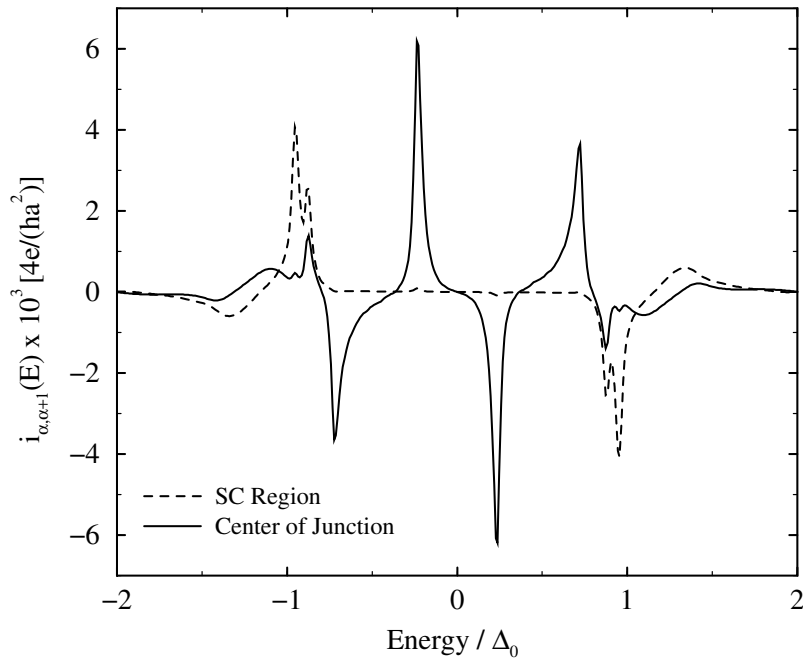
Figure 9. The local current-carrying density of states, $i_{\alpha,\alpha+1}(E)$ at the centre of a Josephson junction (where $\alpha = 0$) and in the superconducting region (where $\alpha = 25$). In this junction $N_b = 20$.

the additional scattering potential, so the anomalous average (and hence the order parameter) exhibits variation more like a step-function, with increasing barrier strength, as expected [51]. We can think of the interfacial scattering as continuously modifying the junction from SNS to SINIS characteristics. Figure 10(b) depicts the effect on the electron density of a positive interfacial potential, which is like a Schottky barrier, since the electronic charge is depleted at the interface. The charge density also exhibits Friedel oscillations away from the barrier (which cannot be seen in approximations that average over short length scales).

5. Charge impurity scattering

We model a barrier region with impurities by using the Falicov–Kimball model, as described in section 2, using equation (1) with $U^{FK} < 0$ and using the self-consistency procedure of equation (31)–(33), as shown in figure 2. We carry out the calculations with an impurity concentration, ρ_{imp} that ranges from 0.01 to 0.2. In the limit of $\rho_{imp} = 0$ there is no scattering in the barrier, and the results correspond to the Hubbard model with $U_b = 0$. Impurities in the barrier region lead to an imaginary part for the frequency-dependent self-energy and, since the lifetime of the quasiparticles at the Fermi surface becomes finite, to a non-Fermi liquid, characteristic of annealed disorder scattering.

The addition of a small number of impurities is seen in figure 11 to decrease the anomalous average in the barrier. The accompanying decrease in both critical current and linear response current, shown in figure 12 by the curves labelled $U^{FK} = -2$, is more severe. Addition of 10% impurities ($\rho_{imp} = 0.10$) leads to a reduction in both current responses to approximately one-third of their initial values, while the anomalous average remains at
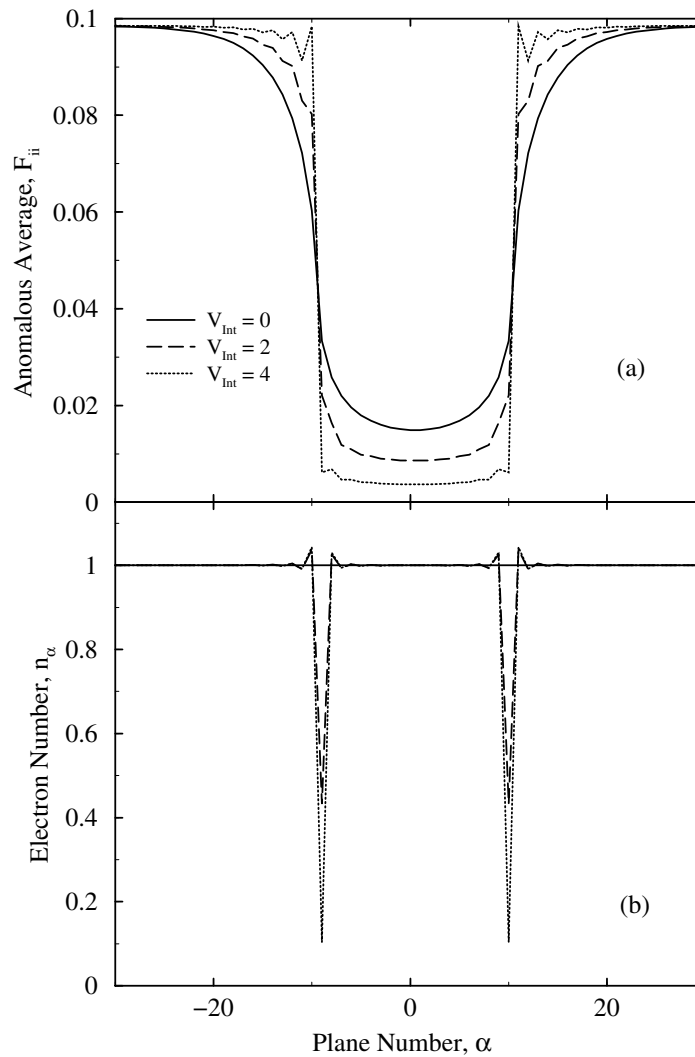
Figure 10. (a) The off-diagonal local Green function, F_{ii}, indicating Friedel oscillations and a reduced proximity effect as the interfacial scattering is increased. (b) Friedel oscillations in the electron density for the same solution.

approximately three-quarters of its original amplitude. Anderson's theorem, which states that non-magnetic impurities do not detract from the superconducting properties of a system only holds for a spatially homogeneous system. Both current flow and the interfaces break the symmetry, so the Josephson junction is inhomogeneous in one dimension, and the effects we observe do not violate Anderson's theorem. General considerations of Green functions in a homogeneous system show that increasing the imaginary part of the electronic self-energy (hence reducing the quasi-particle lifetime) leads to a reduction in supercurrent for a given phase gradient. Hence it is expected that impurities would have a more deleterious effect on current responses than other superconducting properties, which is in the spirit of Anderson's theorem.

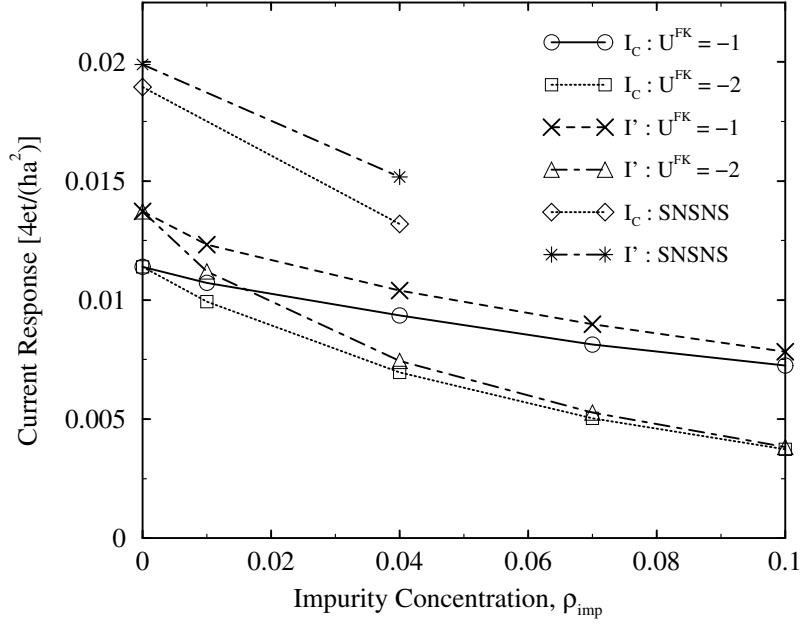We look at the linear response current, I', as a function of temperature for a barrier with
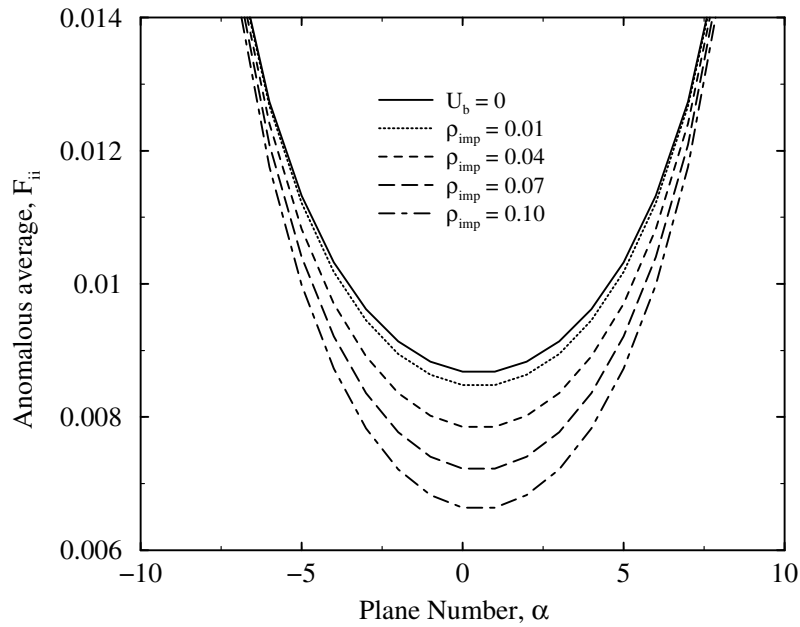
Figure 11. The reduction of the anomalous average, $F_{ii} = F(r_i, r_i, \tau = 0^+)$, for planes near the centre of the barrier, with increasing impurity concentration, ρ_i, and $U^{FK} = -2$.

impurity scattering, in figure 13(a). The critical current remains slightly above zero until the bulk critical temperature, T_c. We can demonstrate one shortcoming of non-self-consistent calculations, by extracting an effective transparency, $\tau = G_N h/2e^2$ of the junction from I' using

$$G_N = I' \left/ \left\{ \frac{\pi \Delta_0(T)}{2e} \tanh \left(\frac{\Delta_0(T)}{2k_B T} \right) \right\} \right. \tag{35}$$

where $\Delta_0(T)$ is the value of the order parameter on the last superconducting plane before the barrier region [23–25]. Whereas simple models of junctions without self-consistency would assume a constant transparency (due to a constant interfacial scattering potential), our results in figure 13(b) demonstrate that a real barrier has lower transparency with increasing temperature. This can be understood from the variation of the self-consistent order parameter, which is reduced to zero within the barrier more rapidly than within the bulk as temperature is increased. Therefore our self-consistent results exhibit a much stronger decrease in critical current with temperature rise than that predicted by more traditional models which only consider Δ within the bulk.

We find self-consistent solutions of a system in the normal state, with no current flow, by setting the order parameter to zero on all planes. These solutions are employed to calculate the resistivity using the Kubo formula, which allows us to consider barrier regions that are correlated. The self-energy of planes outside the barrier contains only a constant real part, as initially we carry out the calculations within the Hartree–Fock approximation. Given the set of local self-energies, the Green functions coupling any two planes are readily found, for any momentum parallel to the planes. We are interested in the longitudinal components in the z-direction (perpendicular to the uniform planes) of the conductivity matrix. We define the conductivity tensor for our effectively one-dimensional system, from the linear current response $I_{\alpha,\alpha+1}$ across a link between two planes, α and $\alpha + 1$, due to an electric field, $E_{\beta,\beta+1}$

Figure 12. The critical current, I_c, and linear response current, I', as a function of charge impurities. Note that I_c and I' decrease as impurities are added to the barrier region. The greater scattering potential of $U^{FK} = -2$ results in greater decrease in current responses, compared to a scattering potential of $U^{FK} = -1$. If superconducting planes are inserted in the middle of the barrier with $U^{FK} = -2$ (SNSNS) the critical current is seen to increase dramatically.

across *all* links between planes β and $\beta + 1$:

$$\sigma_{\alpha,\beta} = \frac{\partial I_{\alpha,\alpha+1}}{\partial E_{\beta,\beta+1}}. \tag{36}$$

We find the conductivity matrix with frequency component, ν, neglecting vertex corrections (which is valid for homogeneous systems in the large dimensional limit) to be

$$\begin{aligned}
\sigma_{\alpha,\beta}(\nu) = \frac{2\hbar}{\nu} \left(\frac{eat}{\hbar}\right)^2 \int_{-\infty}^{\infty} \rho^{2D}(\varepsilon_{xy}) \, d\varepsilon_{xy} \\
\times \int_{-\infty}^{\infty} \frac{d\omega}{2\pi} \{ \text{Im}[G_{\alpha,\beta+1}(\omega, \varepsilon_{xy})] \, \text{Im}[G_{\beta,\alpha+1}(\omega + \nu, \varepsilon_{xy})] \\
+ \text{Im}[G_{\alpha+1,\beta}(\omega, \varepsilon_{xy})] \, \text{Im}[G_{\beta+1,\alpha}(\omega + \nu, \varepsilon_{xy})] \\
- \text{Im}[G_{\alpha,\beta}(\omega, \varepsilon_{xy})] \, \text{Im}[G_{\beta+1,\alpha+1}(\omega + \nu, \varepsilon_{xy})] \\
- \text{Im}[G_{\alpha+1,\beta+1}(\omega, \varepsilon_{xy})] \, \text{Im}[G_{\beta,\alpha}(\omega + \nu, \varepsilon_{xy})]\}[f(\omega) - f(\omega + \nu)] \tag{37}
\end{aligned}$$

where $f(\omega)$ is the Fermi–Dirac distribution function and $\rho^{2D}(\varepsilon_{xy})$ is the two-dimensional tight-binding density of states, used for the sum over momenta parallel to the planes.

We are interested in the zero-frequency response, which is found from the appropriate limit of equation (37):

$$\begin{aligned}
\sigma_{\alpha,\beta}(0) = \frac{-1}{k_B T} \frac{(eat)^2}{\hbar} \int_{-\infty}^{\infty} \rho^{2D}(\varepsilon_{xy}) \, d\varepsilon_{xy} \int_{-\infty}^{\infty} \frac{d\omega}{2\pi} \\
\times [\, \text{Im}[G_{\alpha,\beta+1}(\omega, \varepsilon_{xy})] \, \text{Im}[G_{\beta,\alpha+1}(\omega, \varepsilon_{xy})] \\
- \text{Im}[G_{\alpha,\beta}(\omega, \varepsilon_{xy})] \, \text{Im}[G_{\beta+1,\alpha+1}(\omega, \varepsilon_{xy})]]\,[\cosh^2(\omega/(2k_B T))]^{-1}. \tag{38}
\end{aligned}$$
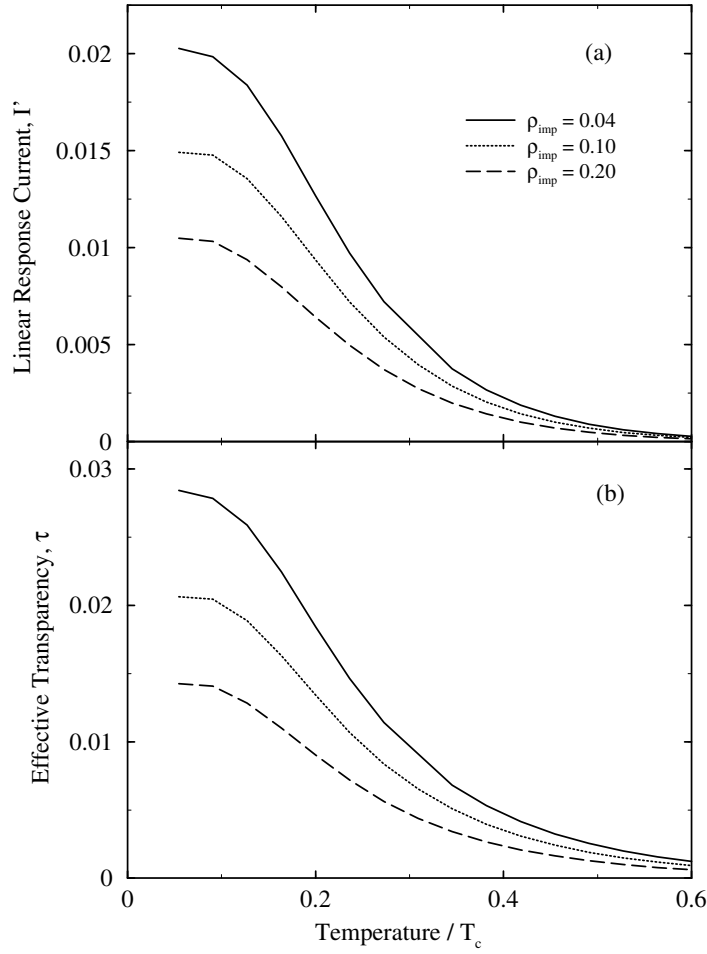
Figure 13. (a) The linear response current, I' (in units $4et/(ha^2)$), as a function of temperature for increasing impurity concentrations in the barrier. (b) The effective transparency as a function of temperature. Note how the effective transparency decays with increasing temperature, shown here for barriers containing impurity scatterers.

When calculating the resistance of the junction, it is important to be aware that for an inhomogeneous 1D system the current flow must be uniform but the electric field is not. The relationship

$$I_{\alpha,\alpha+1} = I_0 = a \sum_{\beta} \sigma_{\alpha,\beta} E_{\beta,\beta+1} \tag{39}$$

leads to

$$E_{\beta,\beta+1} = \frac{1}{a} \sum_{\alpha} (\sigma^{-1})_{\beta,\alpha} I_0 \tag{40}$$

by multiplying on the left by the inverse of the conductivity tensor. The voltage across the junction is the sum of the electric fields across each link, multiplied by the lattice spacing, a, so we obtain the resistance,

$$R_N a^2 = \frac{V}{I_0} = \sum_{\alpha,\beta} (\sigma^{-1})_{\beta,\alpha} \tag{41}$$

given by the sum of components of the inverse conductivity tensor (note that the resistance is actually $R_N a^2$ because we measure the current per unit cell; the factors of a^2 cancel when the $I_c R_N$ product is formed).

It is worthwhile pointing out, that where there is no imaginary part to the self-energy, so there is no quasiparticle decay, the conductivity tensor consists of constant elements, $\sigma_{\alpha,\beta} = \sigma_0$. In such a region, the electric field required to produce a current flow approaches zero as the inverse of the system size, so the local conductivity becomes infinite (that is, the sum of elements in one row of the conductivity tensor increases with system size). However, the voltage drop across the region, given by the product of the electric field and length of perfect lead, remains constant (equal to I_0/σ_0), so the resistance is non-zero [52] (equal to $1/\sigma_0$) while the local resistivity vanishes with large system size. In our calculations, where we neglect any lifetime effects of electrons outside the barrier region (in the Hartree–Fock approximation), there is still a contribution to the resistance of the junction from the 'perfect' leads, but the value of the contribution does not depend on the length of the leads, so it can be thought of as a contact resistance.

Figure 14(a) indicates the variation of junction resistance with impurity concentration in the barrier. The resistance increases linearly with number of scattering sites for the small concentrations calculated, with the slope increasing with the strength of scatterers. The intercept is at a finite resistance, which corresponds to the resistance of an infinitely long, perfectly conducting lead, with conductivity tensor given by $\sigma_{\alpha,\beta} = \sigma_0 \approx 0.625 \times 2e^2/(ha^2)$ (which agrees with the expected Sharvin form of $k_f^2/(4\pi) \times 2e^2/h$ when evaluated at half filling [53]). The resistance calculated for junctions with impurity scattering within the barrier region, does not change when the number of perfectly conducting planes on either side of the barrier is increased from one to 25. Thereafter, numerical instabilities in the matrix inversion process make the calculations unreliable, but we can be confident that the answer already arrived at is the appropriate one for the infinite system.

The product $I_c R_N$ decreases with increasing concentration of impurities in the barrier for the examples shown in figure 14(b). That is, the reduction in critical current is greater than the increase in resistance due to impurity scattering. A system which increases the $I_c R_N$ product has been found experimentally by incorporating an extra (coherent) superconducting region within the barrier [54]. We have examined such an SNSNS or SISIS junction [55], by adapting an SNS structure with 20 barrier planes to replace its central six barrier planes with superconducting material, creating a barrier sandwich of seven normal, six superconducting then seven more normal planes. Both the critical current and linear response current increase by a factor of greater than two, while the normal state resistance is only reduced by 15% from its value for the SNS junction.

6. Conclusions

We have developed an effective method for calculating the equilibrium properties of Josephson junctions. We are able to examine the microscopic details of self-consistently solved systems through local and non-local Green functions. The importance of self-consistency has previously been shown [33–35, 43], so we go beyond standard 'potential barrier' models of junctions to include the effects of spatial correlation and local fluctuations on the self-consistent potentials.

Our results are interpreted in terms of a linear-response current, due to a small phase difference across the junction, as well as the critical current, being the maximum current that a junction can sustain. We find that a self-consistent microscopic determination of the potentials in the system for different phase differences results in current–phase behaviour
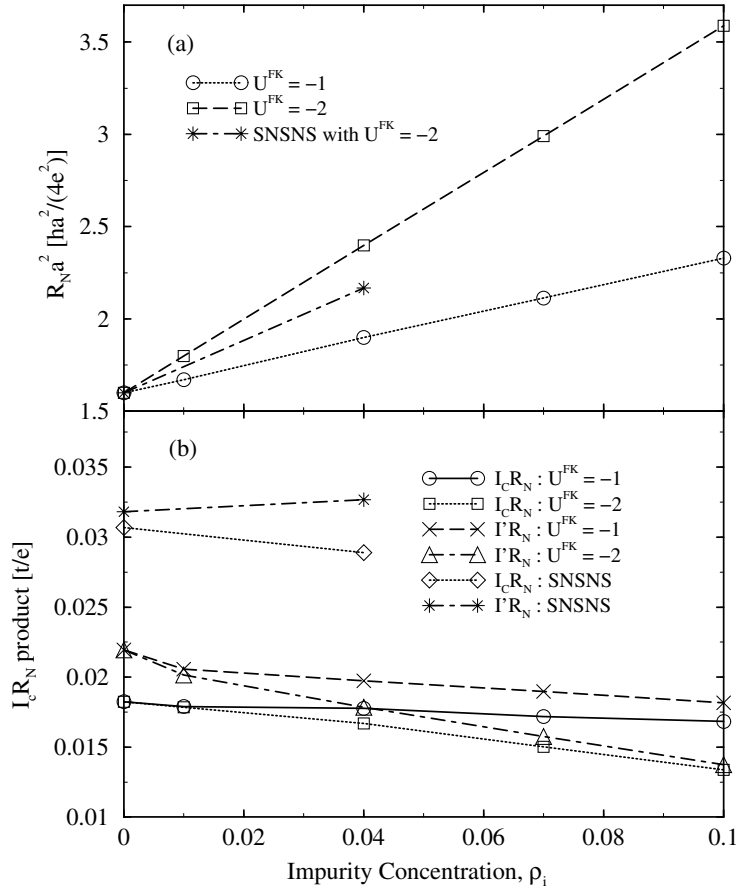
Figure 14. (a) The normal state resistance of a junction versus impurity concentration in the barrier. The scattering potential is greater, $U^{FK} = -2$ for the higher-resistance curve compared to $U^{FK} = -1$ for the lower curve. Insertion of extra planes of superconducting material in the centre of the barrier with $U^{FK} = -2$ (SNSNS) reduces the resistance in this case. (b) The product of normal resistance of a junction with critical current, I_c, and linear response current, I', for the same junctions as (a). Increased figures of merit occur for both clean systems and for the SNSNS structures.

not predictable by standard fixed potential, semiclassical approaches. We study the effects of a number of properties of the barrier material, including its electron–electron interaction potential, its hopping integral and its charge impurity concentration. We also study interfacial scattering potentials, which mimic Schottky barriers and charge accumulation regions, and include barriers with a range of thicknesses. As well as quantifying the change in current response due to such modifications in the barrier, we also depict the alterations in the proximity effect for all cases, and charge variation in the case of an interfacial potential. In future work, we plan to model the charge redistribution at interfaces more realistically, by incorporating a non-local Coulomb potential, which self-consistently determines an effective potential with the charge density for each plane. By such a model, we expect to discover if there is any significant charge redistribution as a junction passes through its superconducting transition, as suggested by Greene's group [56] for Nb–InAs systems.

We have also plotted the local density of states, to observe the bound states which occur

at energies less than the bulk gap, within the barrier region. These states can be both current-carrying Andreev states, or states arising from normal reflections. Their evolution with position and phase variation is seen within our model, as is their contribution to the total current flow when a phase difference is applied. We plan in later work to show how the detailed structure of electronic states, apparent in these equilibrium results, will affect the $I-V$ characteristics of a junction.

We have carried out resistance calculations for junctions with impurities in the barrier, and found that in general the reduction in critical current outweighs the increase in resistance due to charge impurities. We suggest that a junction of the form SNSNS, where a thin layer of superconductor is placed within an normal-metal barrier, can increase the critical current of a junction dramatically, without markedly reducing its resistance. We are in a position to study how more subtle effects involving electronic correlation close to the metal–insulator can affect junction properties.

Our microscopic formulation will be particularly necessary when we proceed to study junctions created with high-temperature superconductor materials. The d-wave symmetry of the order parameter, with its directional dependence, results in behaviour that is not addressed by models utilizing a single transparency. While an appropriate non-local version of the Bogoliubov–de Gennes equations can provide some insight into the properties of d-wave junctions [33, 34], use of the DCA [37, 38] is necessary to tackle the problem from a completely microscopic basis.

Acknowledgments

References

[1] Josephson B D 1962 *Phys. Lett.* **1** 251
[2] McCumber D E 1968 *J. Appl. Phys.* **39** 2503
[3] McCumber D E 1968 *J. Appl. Phys.* **39** 3113
[4] Likharev K K 1984 *Dynamics of Josephson Junctions and Circuits* (London: Gordon and Breach)
[5] Mukhanov O A, Semenov V K and Likharev K K 1987 *IEEE Trans. Magn.* **23** 759
[6] Likharev K K 1999 *Applications of Superconductivity* ed H Weinstock (Dordrecht: Kluwer)
[7] Patel V and Lukens J E 1999 *IEEE Trans. Appl. Supercond.* **9** 3247
[8] Kupriyanov M Yu and Likharev K K 1990 *Sov. Phys.–Usp.* **33** 340
[9] Berkowitz S J, Zhang Y M, Mallison W H, Char K, Terzioglu E and Beasley M R 1996 *Appl. Phys. Lett.* **69** 3257
[10] Miller R, Mallison W H, Kleinsasser A W, Delin K A and Macedo E M 1993 *Appl. Phys. Lett.* **63** 1423
   Kleinsasser A W, Miller R E, Mallison W H and Arnold G B 1994 *Phys. Rev. Lett.* **72** 1738
   Naveh Y, Patel V, Averin D V, Likharev K K and Lukens J E 2000 *Preprint* cond-mat/0006153
[11] Aslamazov L G, Larkin A I and Ovchinnikov Yu N 1968 *Zh. Eksp. Teor. Fiz.* **55** 323 (Engl. transl. *Sov. Phys.–JETP* **28** 171)
   Kuprianov M Yu and Likichev V F 1982 *Fiz. Nizk. Temp.* **9** 548 (Engl. transl. *Sov. J. Low Temp. Phys.* **8** 526)
   Kuprianov M Yu and Likichev V F 1988 *Zh. Eksp. Teor. Fiz.* **94** 139 (Engl. transl. *Sov. Phys.–JETP* **67** 1163)
[12] Barrera A S and Beasley M R 1987 *IEEE Trans. Magn.* **23** 866
[13] Chrestin A, Matsuyama T and Merkt U 1997 *Phys. Rev.* B **55** 8457
[14] Bastian G, Göbel E O, Zorin A B, Schulze H, Niemeyer J, Wiemann T, Bennet M R and Singer K E 1998 *Phys. Rev. Lett.* **81** 1686
[15] Baselmans J J A, Morpurgo A F, van Wees B J and Klapwijk T M 1999 *Nature* **397** 43
   Wilhelm F K, Schön G and Zaikin A D 1998 *Phys. Rev. Lett.* **81** 1682

Baselmans J J A, Morpurgo A F, van Wees B J and Klapwijk T M 1999 *Superlatt. Microstruct.* **25** 973
[16] Heida J P, van Wees B J, Klapwijk T M and Borghs G 1999 *Phys. Rev.* B **60** 13 135
Bastian G 2000 *Phys. Rev.* B **62** 9840
[17] Blonder G E, Tinkham M and Klapwijk T M 1982 *Phys. Rev.* B **25** 4515
[18] Klapwijk T M, Blonder G E and Tinkham M 1982 *Physica* B **109/110** 1657
[19] Arnold G B 1978 *Phys. Rev.* B **17** 3576
[20] Wolf E L and Arnold G B 1982 *Phys. Rep.* **91** 31
[21] Ambegaokar V and Baratoff A 1963 *Phys. Rev. Lett.* **10** 486
[22] Kulik I O and Ome'lyanchuk A N 1978 *Fiz. Nizk. Temp.* **4** 296 (Engl. transl. *Sov. J. Low Temp. Phys.* **4** 142)
[23] Haberkorn W, Knauer H and Richter J 1978 *Phys. Status Solidi* a **47** K161
[24] Furusaki A 1999 *Superlatt. Microstruct.* **25** 809
[25] Tanaka Y and Kashiwaya S 1997 *Phys. Rev.* B **56** 892
[26] Sols F and Ferrer J 1994 *Phys. Rev.* B **49** 15 913
[27] Metzner W and Vollhardt D 1989 *Phys. Rev. Lett.* **62** 324
[28] Jarrell M 1992 *Phys. Rev. Lett.* **69** 168
[29] Freericks J K, Jarrell M and Scalapino D J 1994 *Europhys. Lett.* **25** 37
[30] Freericks J K 1995 *Phys. Rev.* B **50** 403
[31] Potthoff M and Nolting W 1999 *Phys. Rev.* B **59** 2549
[32] Holstein T 1959 *Ann. Phys., NY* **8** 352
[33] Martin A M and Annett J F 1998 *Phys. Rev.* B **57** 8709
[34] Hogan-O'Neill J J, Martin A M and Annett J F 1999 *Phys. Rev.* B **60** 3568
[35] Martin A M and Annett J F 1999 *Superlatt. Microstruct.* **25** 1019
[36] Nambu Y 1960 *Phys. Rev.* **117** 648
[37] Hettler M H, Tahvildar-Zadeh A N, Jarrell M, Prushke Th and Krishnamurthy H R 1998 *Phys. Rev.* B **58** R7475
[38] Maier Th, Jarrell M, Prushke Th and Keller J 2000 *Phys. Rev. Lett.* **85** 1524
[39] Haydock R 1980 *Solid State Physics* vol 35 (New York: Academic)
[40] Haydock R 1984 *The Recursion Method and Its Applications (Springer Series in Solid State Sciences 58)* (Berlin: Springer)
[41] Litak G, Miller P and Györffy B L 1995 *Physica* C **251** 263
[42] Economou E N 1983 *Green Functions in Quantum Physics* (Berlin: Springer) app B
[43] Ovchinnikov Yu N and Barone A 1979 *Sov. Phys.–JETP* **50** 735
Bruder C 1990 *Phys. Rev.* B **41** 4017
Zaitsev A V 1992 *JETP Lett.* **55** 67
Hara J, Ashida M and Nagai K 1993 *Phys. Rev.* B **47** 11 263
Barash Y S, Galaktionov A V and Zaiken A D 1995 *Phys. Rev.* B **52** 665
Xiang T and Wheatley J M 1995 *Phys. Rev.* B **51** 11 721
Miller P and Györffy B L 1995 *J. Phys.: Condens. Matter* **7** 5579
Cannizares J S and Sols F 1995 *J. Phys.: Condens. Matter* **7** L317
Cannizares J S and Sols F 1997 *Phys. Rev.* B **55** 531
Martin A M and Lambert C J 1995 *Phys. Rev.* B **51** 11 799
Martin A M and Lambert C J 1996 *J. Phys.: Condens. Matter* **8** L731
Chang L, Chaudhuri S and Bagwell P F 1996 *Phys. Rev.* B **54** 9399
Riedel R A, Chang L and Bagwell P F 1996 *Phys. Rev.* B **54** 16 082
Dolby P, Seviour R and Lambert C J 2000 *Preprint* cond-mat/0010290
[44] de Gennes P G 1966 *Superconductivity of Metals and Alloys* (New York: Addison-Wesley)
[45] Brandt U and Mielsch C 1989 *Z. Phys.* B **75** 365
[46] Aprili M, Badica E and Greene L H 1999 *Phys. Rev. Lett.* **83** 4630
[47] Fogelström M, Rainer D and Sauls J A 1997 *Phys. Rev. Lett.* **79** 281
Rainer D, Burkhardt H, Fogelström M and Sauls J A 1998 *J. Phys. Chem. Solids* **59** 2040
[48] Šipr O and Györffy B L 1996 *J. Phys. C: Solid State Phys.* **8** 169
[49] Kümmel R, Plehn H and Schüssler U 1996 *Proc. 23rd Int. Conf. on the Physics of Semiconductors* vol 4, p 3387
[50] Thomas M, Blank H-R, Wong K C, Kroemer H and Hu E 1998 *Phys. Rev.* B **58** 11 676
Jacobs A, Kümmel R and Plehn H 1999 *Superlatt. Microstruct.* **25** 669
[51] Likharev K K 1979 *Rev. Mod. Phys.* **51** 101
[52] Zhang X-G and Butler W H 1997 *Phys. Rev.* B **55** 10 308
[53] Sharvin Yu V 1965 *Zh. Eksp. Teor. Phys.* **48** 984 (Engl. transl. *Sov. Phys.–JETP* **21** 655)
[54] Nevirkovets I P, Ketterson J B, and Lomatch S 1999 *Appl. Phys. Lett.* **74** 1624
Nevirkovets I P, Ketterson J B, and Lomatch S 2000 unpublished

[55] Kupriyanov M Yu, Brinkman A, Golubov A A, Siegel M and Rogalla H 1999 *Physica* C **327** 16
Brinkman A, Golubov A A, Rogalla H and Kupriyanov M Yu 1999 *Supercond. Sci. Technol.* **12** 893
Balashov D, Bucholz F-Im, Schulze H, Khabipov M I, Dolata R, Kupriyanov M Yu and Niemeyer J 2000
Supercond. Sci. Technol. **13** 244
Brinkman A and Golubov A A 2000 *Phys. Rev.* B **61** 11 297
[56] Greene L H, Dorsten J F, Roschchin I V, Abeyta A C, Tanzer T A, Kuchler G, Feldmann W L and Bohn P W
1996 *Czech. J. Phys.* **46** 3115
Greene L H 2000 private communication